

Fluorine MR Imaging of Inflammation in Atherosclerotic Plaque in Vivo¹

Ruud B. van Heeswijk, PhD
Maxime Pellegrin, PhD
Ulrich Flögel, PhD
Christine Gonzales, PhD
Jean-François Aubert, MSc
Lucia Mazzolai, MD, PhD
Juerg Schwitter, MD
Matthias Stuber, PhD

¹From the Department of Radiology (R.B.v.H., M.S.), Angiology Service (M.P., J.F.A., L.M.), Cardiology Service (C.G., J.S.), and Cardiac Magnetic Resonance Center (C.G., J.S.), University (UNIL) and University Hospital of Lausanne (CHUV), Rue de Bugnon 46, Lausanne 1011, Switzerland; CardioVascular Magnetic Resonance Research Center (CVMR), Center for Biomedical Imaging (CIBM), Lausanne, Switzerland (R.B.v.H., M.S.); and Department of Cardiovascular Physiology, Heinrich Heine University, Düsseldorf, Germany (U.F.). Received June 12, 2014; revision requested July 15; revision received September 9; accepted September 25; final version accepted October 16. Supported by the Centre d'Imagerie BioMédicale (CIBM) of the UNIL, University of Geneva, University Hospital of Geneva, CHUV, Federal Institute of Technology in Lausanne, and the Leenaards and Jeantet Foundations. R.B.v.H. supported by grants from the Pierre Mercier Foundation and the Swiss Heart Foundation. J.S. supported by the Swiss National Science Foundation (grant 310030_144077) and the Swiss Heart Foundation. Address correspondence to R.B.v.H. (e-mail: ruud.mri@gmail.com).

© RSNA, 2014

Purpose:

To preliminarily test the hypothesis that fluorine 19 (¹⁹F) magnetic resonance (MR) imaging enables the noninvasive in vivo identification of plaque inflammation in a mouse model of atherosclerosis, with histologic findings as the reference standard.

Materials and Methods:

The animal studies were approved by the local animal ethics committee. Perfluorocarbon (PFC) emulsions were injected intravenously in a mouse model of atherosclerosis ($n = 13$), after which ¹⁹F and anatomic MR imaging were performed at the level of the thoracic aorta and its branches at 9.4 T. Four of these animals were imaged repeatedly (at 2–14 days) to determine the optimal detection time. Repeated-measures analysis of variance with a Tukey test was applied to determine if there was a significant change in ¹⁹F signal-to-noise ratio (SNR) of the plaques and liver between the time points. Six animals were injected with a PFC emulsion that also contained a fluorophore. As a control against false-positive results, wild-type mice ($n = 3$) were injected with a PFC emulsion, and atherosclerotic mice were injected with a saline solution ($n = 2$). The animals were sacrificed after the last MR imaging examination, after which high-spatial-resolution ex vivo MR imaging and bright-field and immunofluorescent histologic examination were performed.

Results:

¹⁹F MR signal was detected in vivo in plaques in the aortic arch and its branches. The SNR was found to significantly increase up to day 6 ($P < .001$), and the SNR of all mice at this time point was 13.4 ± 3.3 . The presence of PFC and plaque in the excised vessels was then confirmed both through ex vivo ¹⁹F MR imaging and histologic examination, while no signal was detected in the control animals. Immunofluorescent histologic findings confirmed the presence of PFC in plaque macrophages.

Conclusion:

¹⁹F MR imaging allows the noninvasive in vivo detection of inflammation in atherosclerotic plaques in a mouse model of atherosclerosis and opens up new avenues for both the early detection of vulnerable atherosclerosis and the elucidation of inflammation mechanisms in atherosclerosis.

©RSNA, 2014

In recent years, it has become evident that anatomic predictors, including high plaque burden and the presence of a thin fibrous cap, are by themselves not sufficiently specific to allow prediction of which atherosclerotic plaques will rupture and lead to future events (1). A highly promising and complementary strategy for the identification and definition of plaque vulnerability is the direct visualization of inflammation (2). Indeed, the role of inflammation at all stages of atherosclerosis is now well established (2), and the presence of a macrophage-rich inflammation has been linked to plaque vulnerability (3).

Fluorine 18 (^{18}F) fluorodeoxyglucose positron emission tomography (PET) can, for example, be used for the noninvasive and highly sensitive imaging of inflammation in atherosclerosis through the uptake of the tracer ^{18}F fluorodeoxyglucose in a plaque (4). However, the tracer requires a cyclotron for production, and its radioactivity renders the technique less suitable for long-term disease monitoring. Magnetic resonance (MR) imaging, in combination with the intravenous injection of a contrast agent that is phagocytized by circulating immune cells, can also be used for imaging inflammation in atherosclerosis: Several types of custom-designed gadolinium- and iron oxide-based contrast agents that target inflammation have been described

(5–7) and used for plaque characterization. Iron oxide particles have, for example, been used in humans to detect inflammation in carotid plaques (8) and in the myocardium after infarction (9). However, these techniques have the disadvantage of not being quantitative or being custom designed, or they will likely remain limited to animal studies because of marked regulatory hurdles or concerns related to toxicity and safety. Therefore, despite their promise, a translation to human studies still appears to be distant.

In this proof-of-principle study, we instead propose to use fluorine 19 (^{19}F) MR imaging of injected perfluorocarbons (PFCs) (10,11) for the visualization and quantitative characterization of inflammation in atherosclerotic plaque in vivo. PFCs are inert, nontoxic carbohydrates in which all hydrogen has been replaced with fluorine and of which several types have passed through U.S. Food and Drug Administration trials (12) as blood volume expanders. ^{19}F MR imaging has several distinct advantages over conventional hydrogen 1 (^1H) molecular imaging, which stem from the combination of the facts that the fluorine atoms in the PFCs are imaged directly (in lieu of their effect on their surroundings) and that fluorine is not naturally abundant in the human body at a concentration that is detectable with MR imaging. The ^{19}F signal is therefore highly specific to the injected PFC, and the signal strength is linked to its local quantity, which allows the fluorine concentration to be directly quantified. This means not only that selective angiography with high image contrast (13) can be performed immediately after injection, but also that inflammation in various disease processes such as myocardial infarction (14), arthritis (15), and myocarditis (16) can be visualized with high specificity, as evidenced in various mouse models. Furthermore, post mortem proof-of-principle studies have shown that plaques in the human carotid artery can be labeled and that the PFC nanoparticle concentration can be quantified on a nanomolar scale (17). Thus, the noninvasive ^{19}F MR measurement of the PFC concentration

in vivo may eventually support the quantitative characterization of inflammation in atherosclerosis progression over time and may ultimately be used to better guide and monitor therapy in patients.

For these reasons, we developed and implemented a ^{19}F MR imaging protocol to preliminarily test the hypothesis that ^{19}F MR imaging enables the noninvasive in vivo identification of plaque inflammation in a mouse model of atherosclerosis, with histologic findings as the reference standard.

Materials and Methods

Animal Protocol

The animal studies were approved by the local animal ethics committee. Fifteen 8-week-old male apolipoprotein E knockout (ApoE $^{-/-}$) mice (B6.129P2-ApoE $^{-/-}$ tm1Unc) and three C57Bl/6 wild-type (WT) mice (all from Charles River Laboratories, L'Arbresle, France) were fed a high-fat diet (20% milk butter and 0.15% cholesterol, Western Diet U8958 version 52; Safe Diets, Augy, France) for 12 weeks to exacerbate atherosclerosis development and to keep experimental conditions as similar as

Advances in Knowledge

- Fluorine MR imaging of an injected perfluorocarbon (PFC) emulsion can be used to detect inflammation in atherosclerotic plaque in vivo.
- Injected PFC emulsions are internalized by macrophages as well as other immune cells in atherosclerotic plaque in apolipoprotein E knockout mice.
- Injected PFC emulsions build up over several days after injection, which results in an optimal imaging time point well after the emulsion has cleared from the bloodstream.

Published online before print

10.1148/radiol.14141371 Content codes: MR VA

Radiology 2015; 000:1–9

Abbreviations:

ApoE $^{-/-}$ = apolipoprotein E knockout
 FITC = fluorescein isothiocyanate
 PFC = perfluorocarbon
 SNR = signal-to-noise ratio
 WT = wild type
 3D = three-dimensional

Author contributions:

Guarantors of integrity of entire study, R.B.v.H., C.G., M.S.; study concepts/study design or data acquisition or data analysis/interpretation, all authors; manuscript drafting or manuscript revision for important intellectual content, all authors; approval of final version of submitted manuscript, all authors; agrees to ensure any questions related to the work are appropriately resolved, all authors; literature research, R.B.v.H., M.P., L.M., J.S., M.S.; clinical studies, M.P.; experimental studies, R.B.v.H., M.P., U.F., C.G., J.F.A., L.M.; statistical analysis, R.B.v.H., M.P.; and manuscript editing, R.B.v.H., M.P., U.F., C.G., L.M., J.S., M.S.

Conflicts of interest are listed at the end of this article.

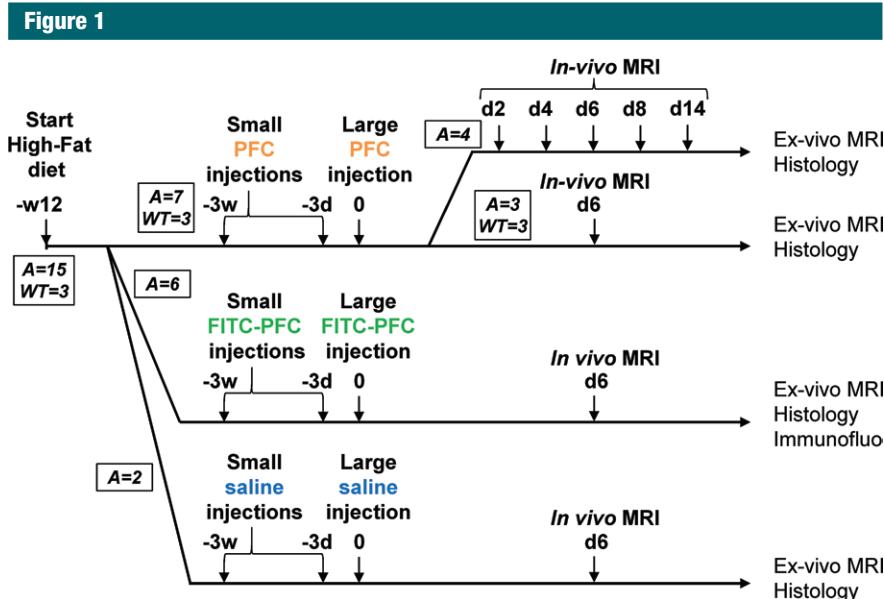


Figure 1: Schematic overview of the experiments. All mice ($A = \text{ApoE}^{-/-}$, $WT = \text{WT control}$) followed a high-fat diet, 12 weeks after which they were serially injected with PFC, FITC-PFC, or saline. They then underwent serial MR imaging or a single session of MR imaging 6 days after the last injection. Immediately after the last MR imaging session they were euthanized, which was followed by ex vivo MR imaging and histologic examination. Immunofluorescent histologic examination (*Immunofluo*) was then performed on the aortas of the FITC-PFC-injected mice.

possible for the control mice (Fig 1). $\text{ApoE}^{-/-}$ mice were selected, since this is a well-established model for atherosclerosis research and since the size of their aortas is on the same order of magnitude as that of human coronary arteries. A PFC emulsion based on 10% wt/vol perfluoro-15-crown-5 ether was prepared in-house as described previously (14). The emulsion contains nanoparticles with a mean size of 130 nm, produces a single spectral line at -92.8 ppm (18), and contains approximately 8×10^9 ^{19}F atoms per nanoparticle. A PFC injection scheme that was estimated to maximize the PFC loading in the plaque at the time of MR imaging was experimentally developed: Every 3 days during weeks 10–12 after the start of the diet, seven $\text{ApoE}^{-/-}$ mice and the three WT mice received 100- μL tail-vein injections. The rationale for these empirically chosen small injections was to inject a small but still substantial volume with a sufficiently large time interval to allow the body to accommodate for the increase in blood volume. After the 12 weeks, the animals received a

large PFC injection of 500 μL . Six more $\text{ApoE}^{-/-}$ mice received the same injection protocol with fluorescein isothiocyanate (FITC) PFC (15), an emulsion to which the fluorophore FITC was added to perform histologic validation with fluorescence microscopy. Two control $\text{ApoE}^{-/-}$ mice were injected with saline to characterize the ^{19}F signal that does not originate from the injected PFC—that is, the anesthetic isoflurane (which is known to be absorbed in the subcutaneous fat [19]).

In Vivo MR Imaging

First, MR images were obtained in four PFC-injected $\text{ApoE}^{-/-}$ mice on day 2, 4, 6, 8, and 14 after the last injection to determine the optimal time delay between injection and imaging, since the specific pharmacokinetics of this PFC in atherosclerotic plaque are unknown. The remaining three PFC-injected animals, as well as the six FITC-PFC-injected animals, the two saline-injected $\text{ApoE}^{-/-}$ mice, and the three WT controls underwent imaging 6 days after the last injection.

All MR experiments were performed in a 9.4-T horizontal bore animal spectrometer (Varian, Palo Alto, Calif). Animals underwent isoflurane anesthesia (4% in air for induction, followed by 2% in a mixture of 60% oxygen and 40% air). Electrocardiographic electrodes were applied to the paws, and the animals were placed in a dedicated holder on top of a respiration pillow and a custom-designed 18-mm-diameter quadrature surface coil that is tunable to both the ^1H and ^{19}F resonance frequencies. The body temperature was monitored with a rectal probe (SA Instruments, Stony Brook, NY) and kept constant at $37.0^\circ\text{C} \pm 0.5$ by using tubing with circulating warm water.

Segmented bright-blood ^1H gradient echo images (field of view, 30×30 mm 2 ; section thickness, 1 mm; six sections acquired; 128×128 matrix; resolution, $0.23 \times 0.23 \times 1$ mm 3 or 55 nL; four signals acquired; repetition time msec/echo time msec, 3.9/1.9; acquisition time, approximately 8 minutes) were acquired at the level of the thoracic aorta and its branches in various orientations (sagittal, transverse, and oblique coronal to follow the aorta) for anatomic localization. This ^1H gradient-echo pulse sequence was triggered with both electrocardiography and respiration (SA Instruments) to compensate for motion. This was followed by non-triggered multisection ^{19}F turbo spin-echo imaging (64×64 matrix, resolution of $0.47 \times 0.47 \times 1$ mm 3 or 220 nL, 360 signals acquired, 1250/4.2, echo train length of 16, and acquisition time of 30 minutes) at the same anatomic level. Here, the signal averaging helped suppress any motion artifacts.

MR image analysis was performed by R.B.v.H. (with 8 years of experience with small-animal MR imaging). Signal-to-noise ratio (SNR) levels were established for several regions to gain insight into the time course of signal change and the maximal signal strength that could be obtained with the technique (not to quantify concentrations). The SNR of a region of interest was defined as the average signal in the region of interest divided by the standard deviation of a 10×5 -mm 2 region of noise outside

the mouse body. By using ^1H MR images for visual coregistration, the SNR of ^{19}F signal in vessels suspected of having atherosclerotic plaque as well as the liver was quantified in the unprocessed ^{19}F images of the mice injected with PFC. All ^{19}F images were then postprocessed for visualization with a 3-pixel-diameter Gaussian filter and interpolated twice, after which they were thresholded at three times the unprocessed background standard deviation and directly fused with the ^1H images in Matlab (Mathworks, Natick, Mass).

In the mice that underwent imaging on multiple days, the ^{19}F SNR of the aortic arch and its branches, as well as that of the liver, were compared between the different days to determine the optimal time point after which the SNR no longer increases significantly in the aortic arch and its branches.

Ex Vivo Imaging

All animals were euthanized by means of pentobarbital overdose after the in vivo MR imaging. Euthanized mice were perfused at physiologic pressure with phosphate-buffered saline and then with buffered formaldehyde via an arterial catheter. The aortic arch was excised and photographed en face with a digital camera (Coolpix; Nikon, Düsseldorf, Germany) for visual identification of plaques and their location by M.P. and J.F.A. (with 10 and 15 years of experience with mouse dissection and histologic analysis, respectively). Subsequently, specimens were stored in a 2% formaldehyde-in-saline solution and placed in the MR imaging unit. To ascertain that the ^{19}F signals originated from the aorta and not from adjacent tissue or other signal sources at the obtainable SNR level in vivo, the same multisection ^1H gradient-echo and ^{19}F turbo spin-echo sequences as those used for the in vivo MR imaging were then performed, but with a 128×128 matrix and 2880 signals acquired for the ^{19}F sequence. For high-spatial-resolution three-dimensional (3D) visualization of the ^{19}F signal in the aorta, 3D ^1H (field of view, $20 \times 15 \times 10 \text{ mm}^3$; $128 \times 128 \times 64$ matrix; resolution, $0.16 \times 0.12 \times 0.16 \text{ mm}^3$ or 2.86 nL ; eight signals averaged; $80/2.6$;

and acquisition time, 1.5 hours) and ^{19}F ($64 \times 64 \times 32$ matrix; resolution, $0.31 \times 0.23 \times 0.31 \text{ mm}^3$ or 22.9 nL ; 640 signals averaged; $40/1.5$; acquisition time, 14.5 hours) gradient-echo pulse sequences at the same anatomic location were used. Both data sets were then interpolated to a $512 \times 512 \times 256$ matrix size, semi-automatically segmented, and fused in Matlab (Mathworks).

Histologic Examination

For two mice in each group, the aortic arches and branching vessels were embedded in paraffin, and 3- μm -thick sections were obtained at the level of plaques in the brachiocephalic artery. Movat pentachrome staining (20) of locations where ^{19}F signal was observed was then performed for plaque characterization and reference-standard comparison with ^{19}F MR imaging by M.P. and R.B.v.H. Here, blue indicates ground substance, blue-black suggests nuclei and elastic fibers, red relates to muscle, intense red represents fibrin, and green-yellow designates collagen and reticulin fibers.

Immunofluorescent staining was performed (by C.G., with 9 years of experience with immunohistochemistry) in adjacent sections to confirm the presence of FITC PFC in macrophages. Sections were selectively immunostained for mouse macrophages with antimouse Mac-2 antibody (rat monoclonal antibody, Cedarlane, Burlington, Canada). The FITC signal was amplified by using an anti-FITC antibody (rabbit polyclonal antibody; Invitrogen, Grand Island, NY) to avoid nonspecific autofluorescence contamination. Mac-2 and FITC were visualized with Alexa 594 and Alexa 488 conjugated antibodies (Molecular Probes, Eugene, Oregon), respectively. Nuclei were stained with 4',6-diamidino-2-phenylindole (Molecular Probes). Imaging was performed by using an Axiovision fluorescence microscope (Carl Zeiss, Oberkochen, Germany).

Statistical Analyses

Values were represented as means \pm 1 standard deviation. Repeated-measures analysis of variance with a post hoc Tukey test was applied to determine

if there was a significant change in ^{19}F SNR of the plaques or liver between subsequent imaging days. A *P* value less than .05 was considered to indicate a statistically significant difference.

Results

In Vivo Detection of PFC in the Aorta and Its Branches with ^{19}F MR Imaging

Small patches of ^{19}F signal were observed in regions where atherosclerotic plaques commonly occur in the ApoE $^{-/-}$ mouse model (21), such as the aortic arch, the carotid arteries, and the brachiocephalic artery (Fig 2, A, B). Marked ^{19}F signal was furthermore observed in several repositories of immune cells, such as the liver (Kupffer cells), lymph nodes, and spinal cord. Signal was also observed in subcutaneous fat, but control experiments with ApoE $^{-/-}$ mice that were injected with saline instead of PFC confirmed that this was isoflurane, which accumulates exclusively in subcutaneous fat (19). No ^{19}F signal was observed in the descending thoracic aorta of any of the mice. PFC-injected WT control mice showed no ^{19}F signal at the level of the aorta or its branches. However, signal was observed in the liver, lymph nodes, and subcutaneous fat, as expected.

^{19}F MR images of the PFC-injected ApoE $^{-/-}$ mice that underwent imaging multiple times demonstrated that the ^{19}F SNR in the aorta and its branches no longer significantly increases after day 6, when a 117% SNR enhancement ($P < .001$) versus that of day 2 was observed (Fig 2, C). Day 6 after PFC injection was therefore deemed the optimal imaging day for the protocol. The mean ^{19}F SNR of all PFC-injected ApoE $^{-/-}$ mice on day 6 was 13.4 ± 3.3 (range, 9.3–17.6) in the aortic arch and its branches, while the highest SNR (117 ± 22) was found in the liver on day 8 ($P = .005$, Fig 2, D).

Ex Vivo Confirmation of PFC in Plaque

Plaques that were identified on the photographs (Fig 3, A) were also individually identified on the ex vivo MR images (Fig 3, B), which confirmed that the

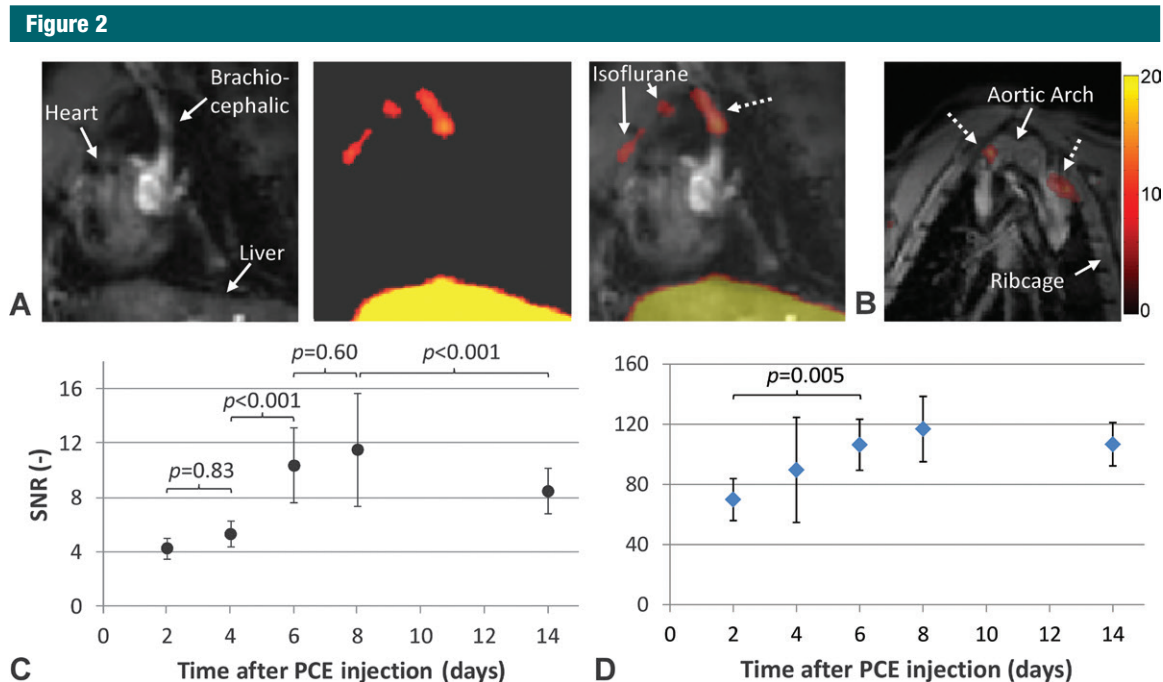


Figure 2: *A*, Sagittal in vivo ^{19}F and ^1H MR images of atherosclerotic plaque in $\text{ApoE}^{-/-}$ mice. The “hot-iron” scale is used for the ^{19}F SNR level (inset color bar), which is overlaid on the anatomic ^1H images in gray scale. The MR images were obtained through the liver, the side of the heart, and the brachiocephalic artery. The left panel shows the anatomic ^1H image, the middle panel the processed ^{19}F image, and the right panel the fusion of the two. The dotted arrow indicates the atherosclerotic plaque, which was later confirmed by means of ex vivo histologic examination, but signal intensity can also be observed in the liver because of the Kupffer cells taking up PFC and in the subcutaneous fat from the anesthetic isoflurane. *B*, In another animal, an oblique coronal $^{19}\text{F}/^1\text{H}$ fusion MR image shows two plaques in the aortic arch. *C*, Plot of ^{19}F SNR in the plaques of the group of mice that underwent imaging multiple times demonstrates that the SNR does not significantly change after day 6. *D*, Plot of ^{19}F SNR in the liver shows a similar trend as that in the plaques, albeit with a higher SNR. The SNR was not significantly different among consecutive days, and only the increase from day 2 to day 6 was statistically significant in the liver when all days were compared. *PCE* = perfluoro-15-crown-5 ether.

source of the ^{19}F signal was within the aortas. Three-dimensional visualizations of segmented high-spatial-resolution 3D MR imaging further illustrated the location of the PFC deposits in the vessel wall (Fig 3, C).

Co-localization of PFC and Immune Cells

Movat pentachrome staining confirmed the presence of intermediate plaques at the locations of the ^{19}F signal, consistent with the disease model (Fig 4, A, B). Subsequent immunofluorescent staining for mouse macrophages (through Mac-2) and PFC (through FITC) demonstrated the presence of PFC in plaque macrophages through the colocalization of the fluorescent signals, although not all PFC was contained in macrophages (Fig 4, C–E). Importantly, immunofluorescent staining showed

no macrophage or ^{19}F signal in the WT control mice, while in the control $\text{ApoE}^{-/-}$ mice that were injected with saline—that is, those without PFC—only a macrophage signal was detected at histologic examination.

Discussion

This study demonstrated the feasibility of the in vivo ^{19}F MR imaging detection of inflammation in atherosclerotic plaque, with ex vivo imaging and immunofluorescent histologic findings as the reference standard. The technique differs from previously described MR imaging techniques in that the PFC does not indirectly modulate an existing signal like iron oxide (22) or gadolinium (23) nanoparticles do but directly generates the ^{19}F signal itself without the

presence of background signals. This allows for very high specificity and the ultimate possibility of direct SNR quantification that is linearly related to the present quantity of PFC (17). Since there is no need for potentially harmful ionizing radiation, and since the PFC particles are considered safe (several variants have been studied in clinical trials) (24), ^{19}F MR imaging appears to be well positioned for translation into the clinical setting, where it may be used to monitor the response of an individual patient to a therapy designed to decelerate, halt, or reverse plaque progression.

Our study had limitations. The PFC concentration itself was not quantified in this study, since the effects of motion compensation through averaging on the signal strength has not been studied

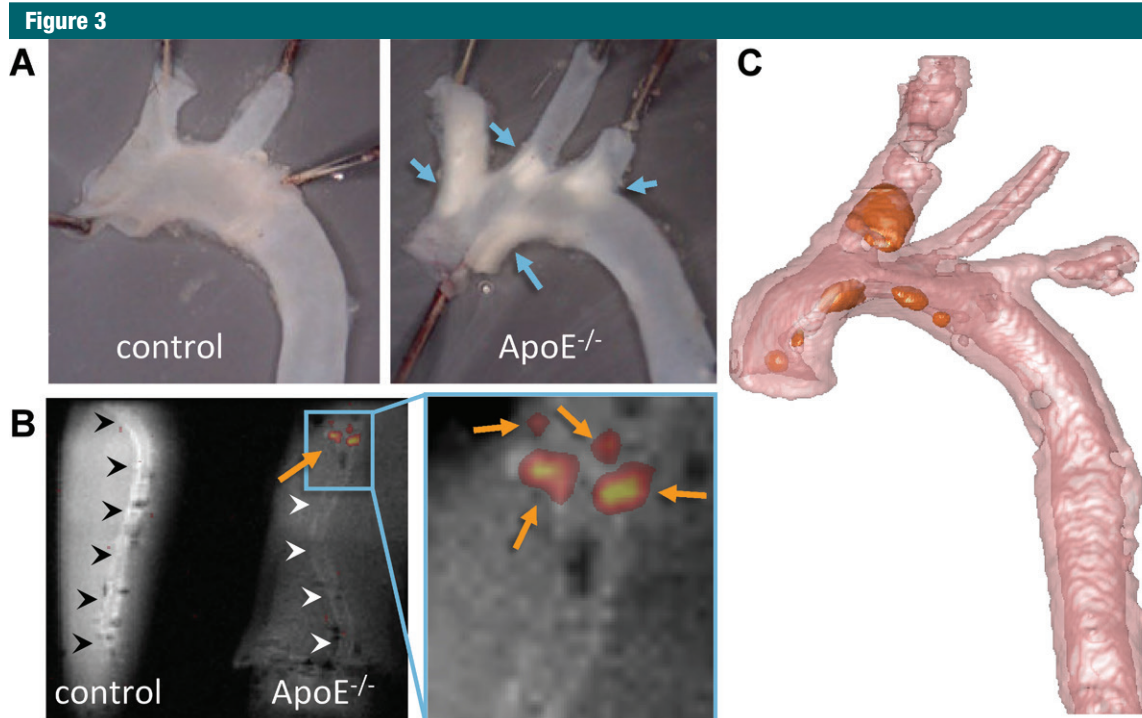


Figure 3: Ex vivo visualization of atherosclerotic plaques in mouse aortic arches. *A*, En face photographs of excised aortic arches and their branching vessels of a WT control mouse and an ApoE^{-/-} mouse. Atherosclerotic plaques are observed as white patches in the ApoE^{-/-} mouse aorta (arrows). *B*, ¹⁹F/¹H MR image of the same control and ApoE^{-/-} mouse aortas (arrowheads) shows ¹⁹F signal intensity in a similar pattern (arrows) as the plaques in the photographs, while no ¹⁹F signal intensity is observed in the control mouse aorta. Small dark patches on the ¹H images are caused by trapped microscopic air bubbles. *C*, High-spatial-resolution 3D rendering of an aorta and its ¹⁹F signal intensity are shown in a different mouse. Both the inner and outer surface of the aortic wall have been visualized in transparent pink, while the ¹⁹F signal intensity in orange can be seen to be located on the inner surface of the aortic arch and the brachiocephalic artery.

and since the loading of the used surface radiofrequency coil would need to be determined for each mouse individually (25). A minimum amount of labeled immune cells that are needed for the signal to be detected is therefore difficult to establish, although a detection limit of this type of imaging protocol was previously reported to be approximately 400 cells per voxel (14). Considering that no ¹⁹F signal was detected in the descending aorta and that smaller plaques commonly occur there (26), an improved sensitivity might be needed to detect very small plaque formations. Fortunately, several avenues are available for future improvements, such as an optimized PFC administration scheme; a higher PFC load in the emulsion (safe formulations with up to 30% instead of the 10% used here have been reported [27]); the implementation of novel image reconstruction

methods, such as compressed sensing (28); or the postformulation addition of a targeting ligand (29). Furthermore, the exact correlation of the ¹⁹F MR signal with the macrophage load as can be determined through histologic examination should be established, while the exact populations that internalize PFC could be investigated by means of flow cytometry.

We found that 6 days after the last injection was the optimal time point to perform imaging. This time point most likely results from a combination of both the number and spread of the injection series and the composition and clearance rate of the PFC emulsion. However, we did not further optimize the injection scheme for this proof-of-principle study. Possible sources of the increase in PFC over time are the liver and spleen, where the sequestered immune cells retain PFC for several weeks

(30). The slow increase and decrease of ¹⁹F signal over time in the liver is furthermore consistent with previous observations for perfluoro-15-crown-5 ether (30).

Immunofluorescent histologic results further demonstrated PFC absorption by cell types other than macrophages, which is in line with the findings of other studies (16,31). However, since the FITC is covalently linked only to the phospholipids in the emulsion and not to the perfluoro-15-crown-5 ether, it should be noted that we cannot be certain that these two components of the FITC PFC are still 100% associated with one another, especially at the later imaging time points. Furthermore, contrary to nanoparticles that exhibit a certain targeting ligand, it currently remains to be elucidated how exactly the “passive” nanoparticles used in this study

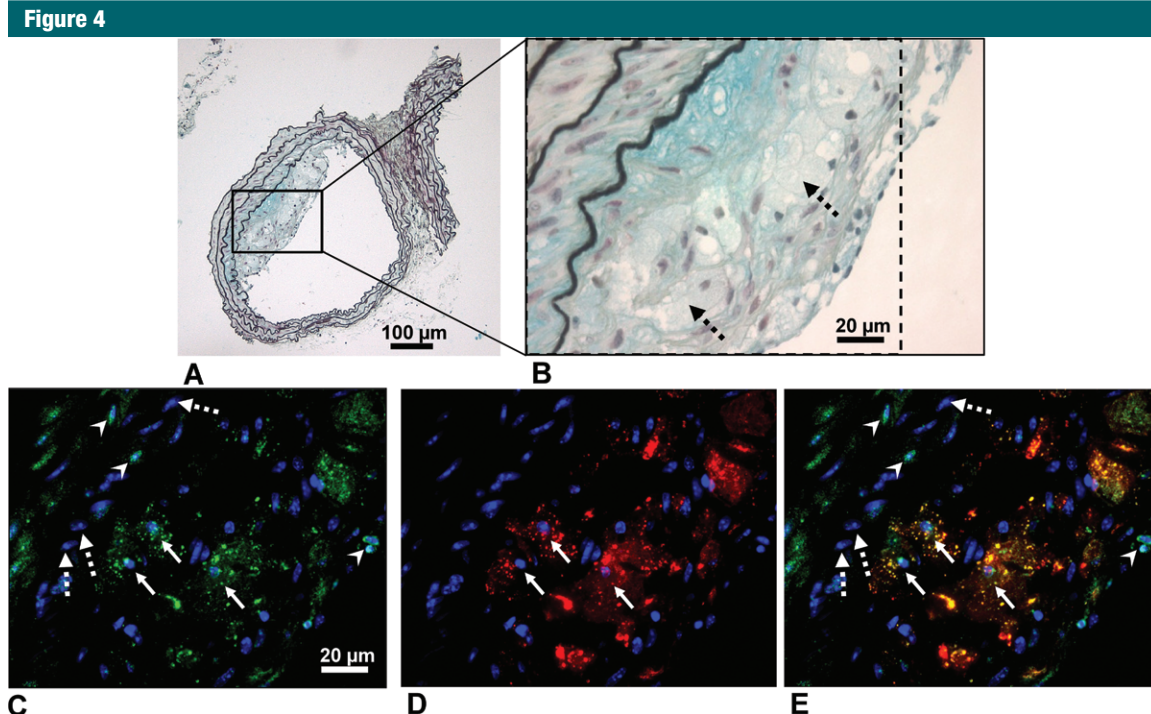


Figure 4: Histologic images show an intermediate-stage atherosclerotic plaque in a brachiocephalic artery. *A, B*, Movat pentachrome staining (original magnification for *A*, $\times 10$; original magnification for *B*, $\times 60$) shows that the plaque is characterized by the presence of macrophage foam cells (black dotted arrows on *B*), a necrotic core (in blue), and a thin fibrous cap. This plaque is located on the inner surface, as also observed in the 3D renderings, and occupies approximately $(42/152) \times 10^3 \mu\text{m}^2 = 28\%$ of the vessel lumen area. *C, D*, Immunofluorescence staining (original magnification, $\times 63$) of the same region of the plaque (area inside the dashed box on *B*) demonstrates the presence of PFC (FITC in green) and macrophages (Mac-2 in red) in the plaque. Blue indicates cellular nuclei (from 4',6-diamidino-2-phenylindole). *E*, Merged picture of *C* and *D* (original magnification, $\times 63$) demonstrates that most of the PFC is contained within the macrophages (solid arrows on *C–E*). Cells that are not macrophages that absorbed PFC (arrowheads on *C* and *E*) and cells that are not macrophages and did not absorb PFC (dotted arrows on *C* and *E*) can also be observed.

migrate into the plaque. They might be phagocytized by monocytes in the bloodstream that then migrate to the plaque, or they might diffuse through leaky endothelium via the vasa vasorum or directly into the plaque or by a combination of the above. Should a higher sensitivity be obtained by using advanced methods, such mechanisms could be studied in-depth by following the fate of injected specific immune cell populations that are labeled in vitro (32), which would result in valuable new insights into the mechanisms of cell turnover in atherosclerosis.

In the clinical realm, the most established noninvasive atherosclerosis inflammation imaging technique is currently PET of the injected radioactive tracer ^{18}F fluorodeoxyglucose, which is used to detect an increase in plaque

metabolism and has a very high sensitivity, while it also has the advantage of being quantifiable (33). However, the spatial resolution of PET is inherently quite low, it requires a nearby cyclotron, and, to provide an anatomic reference for such small structures as atherosclerotic plaques, it needs to be overlaid on an anatomic computed tomographic (CT) or MR image. CT involves another dose of potentially harmful ionizing radiation and renders the technique less suitable for monitoring disease progression or therapy, while for the ^{19}F MR imaging technique described here, anatomic ^1H images are readily available for coregistration.

Given that 0.5 L of PFC has already been injected as a blood volume expander in humans (12), the dosage in this study was deliberately chosen to

be high to maximize the ^{19}F signal and to ensure visualization of the plaque inflammation. However, a dose optimization or a study of the absorption kinetics has not yet been performed, and it can therefore be hypothesized that fewer (perhaps even a single) or smaller injections may achieve similar plaque ^{19}F loading. It should also be noted that because of the slow clearance kinetics of the crown ether used in this study (30), other PFCs might be more suitable for human applications. PFCs with a single resonance, such as perfluoropolyether (34) or “Perfecta” (35), might have different kinetics and allow for fewer injections, although this remains to be tested. Furthermore, given that the voxel size in humans is often more than two orders of magnitude larger than that used in

mice here (up to $2 \times 2 \times 8 \text{ mm}^3$ or $32 \mu\text{L}$ vs $0.22 \mu\text{L}$ used in this study), a smaller dose may in fact be sufficient for initial plaque macrophage visualization in human carotid arteries. A quick calculation suggests that scaling from 2.5 mL total blood volume in mice to 5 L in humans with 10 times larger voxel size results in a 100-mL slow infusion volume (while the smaller injections translate to 20 mL), but this remains to be investigated and optimized. Since the detection limit of ^{19}F is on the order of $400 \mu\text{mol/L}$ for gradient-echo MR imaging (13), a detection limit down to at least 13 nmol per voxel might be expected in humans. This relative signal increase could equally be used to improve the sensitivity and to reduce the ^{19}F MR imaging time.

In conclusion, we provided a preliminary account of the utility of a safe fluorine MR imaging technique for the in vivo visualization of inflammation in atherosclerosis. This opens a new avenue for research and discovery in atherosclerosis on the one hand and may ultimately provide a tool to better help guide and monitor therapy in patients at risk for atherosclerosis or those with documented atherosclerosis on the other hand.

Acknowledgments: We thank Karima Bouzourene, MSc, for her expertise and assistance with the histologic examinations and Simone Coppo, MSc, for the 3D visualization.

Disclosures of Conflicts of Interest: R.B.v.H. disclosed no relevant relationships. M.P. disclosed no relevant relationships. U.F. disclosed no relevant relationships. C.G. disclosed no relevant relationships. J.E.A. disclosed no relevant relationships. L.M. disclosed no relevant relationships. J.S. Activities related to the present article: disclosed no relevant relationships. Activities not related to the present article: author received a research grant from Bracco, and the hospital received a research grant and consulting fees from Medtronic. Other relationships: disclosed no relevant relationships. M.S. disclosed no relevant relationships.

References

- Stone GW, Maehara A, Lansky AJ, et al. A prospective natural-history study of coronary atherosclerosis. *N Engl J Med* 2011;364(3):226–235.
- Libby P. Inflammation in atherosclerosis. *Nature* 2002;420(6917):868–874.
- Swirski FK, Pittet MJ, Kircher MF, et al. Monocyte accumulation in mouse atherogenesis is progressive and proportional to extent of disease. *Proc Natl Acad Sci U S A* 2006;103(27):10340–10345.
- Orbay H, Hong H, Zhang Y, Cai W. Positron emission tomography imaging of atherosclerosis. *Theranostics* 2013;3(11):894–902.
- Leuschner F, Nahrendorf M. Molecular imaging of coronary atherosclerosis and myocardial infarction: considerations for the bench and perspectives for the clinic. *Circ Res* 2011;108(5):593–606.
- Te Boekhorst BC, van Tilborg GA, Strijkers GJ, Nicolay K. Molecular MRI of inflammation in atherosclerosis. *Curr Cardiovasc Imaging Rep* 2012;5(1):60–68.
- Ruehm SG, Corot C, Vogt P, Kolb S, Debatin JF. Magnetic resonance imaging of atherosclerotic plaque with ultrasmall superparamagnetic particles of iron oxide in hyperlipidemic rabbits. *Circulation* 2001;103(3):415–422.
- Tang TY, Howarth SP, Miller SR, et al. The ATHEROMA (Atorvastatin Therapy: Effects on Reduction of Macrophage Activity) Study. Evaluation using ultrasmall superparamagnetic iron oxide-enhanced magnetic resonance imaging in carotid disease. *J Am Coll Cardiol* 2009;53(22):2039–2050.
- Alam SR, Shah AS, Richards J, et al. Ultrasmall superparamagnetic particles of iron oxide in patients with acute myocardial infarction: early clinical experience. *Circ Cardiovasc Imaging* 2012;5(5):559–565.
- Ruiz-Cabello J, Barnett BP, Bottomley PA, Bulte JW. Fluorine (^{19}F) MRS and MRI in biomedicine. *NMR Biomed* 2011;24(2):114–129.
- Schwittler J. Extending the frontiers of cardiac magnetic resonance. *Circulation* 2008;118(2):109–112.
- Riess JG. Perfluorocarbon-based oxygen delivery. *Artif Cells Blood Substit Immobil Biotechnol* 2006;34(6):567–580.
- van Heeswijk RB, Pilloud Y, Flögel U, Schwittler J, Stuber M. Fluorine-19 magnetic resonance angiography of the mouse. *PLoS ONE* 2012;7(7):e42236.
- Flögel U, Ding Z, Hardung H, et al. In vivo monitoring of inflammation after cardiac and cerebral ischemia by fluorine magnetic resonance imaging. *Circulation* 2008;118(2):140–148.
- Flögel U, Burghoff S, van Lent PL, et al. Selective activation of adenosine A2A receptors on immune cells by a CD73-dependent prodrug suppresses joint inflammation in experimental rheumatoid arthritis. *Sci Transl Med* 2012;4(146):ra108.
- van Heeswijk RB, De Blois J, Kania G, et al. Selective in vivo visualization of immune-cell infiltration in a mouse model of autoimmune myocarditis by fluorine-19 cardiac magnetic resonance. *Circ Cardiovasc Imaging* 2013;6(2):277–284.
- Morawski AM, Winter PM, Yu X, et al. Quantitative “magnetic resonance immunohistochemistry” with ligand-targeted (^{19}F) nanoparticles. *Magn Reson Med* 2004;52(6):1255–1262.
- Kadayakkara DK, Damodaran K, Hitchens TK, Bulte JW, Ahrens ET. (^{19}F) spin-lattice relaxation of perfluoropolyethers: dependence on temperature and magnetic field strength (7.0–14.1T). *J Magn Reson* 2014;242:18–22.
- Eger EI 2nd, Saidman LJ. Illustrations of inhaled anesthetic uptake, including intertissue diffusion to and from fat. *Anesth Analg* 2005;100(4):1020–1033.
- Menu P, Pellegrin M, Aubert JF, et al. Atherosclerosis in ApoE-deficient mice progresses independently of the NLRP3 inflammasome. *Cell Death Dis* 2011;2:e137.
- Weinreb DB, Aguinaldo JG, Feig JE, Fisher EA, Fayad ZA. Non-invasive MRI of mouse models of atherosclerosis. *NMR Biomed* 2007;20(3):256–264.
- Korosoglou G, Weiss RG, Kedziorek DA, et al. Noninvasive detection of macrophage-rich atherosclerotic plaque in hyperlipidemic rabbits using “positive contrast” magnetic resonance imaging. *J Am Coll Cardiol* 2008;52(6):483–491.
- Amirbekian V, Lipinski MJ, Briley-Saebo KC, et al. Detecting and assessing macrophages in vivo to evaluate atherosclerosis noninvasively using molecular MRI. *Proc Natl Acad Sci U S A* 2007;104(3):961–966.
- Leese PT, Noveck RJ, Shorr JS, Woods CM, Flaim KE, Keipert PE. Randomized safety studies of intravenous perflubron emulsion. I. Effects on coagulation function in healthy volunteers. *Anesth Analg* 2000;91(4):804–811.
- Gruetter R, Prolla TA, Shulman RG. ^{13}C NMR visibility of rabbit muscle glycogen in vivo. *Magn Reson Med* 1991;20(2):327–332.
- Nakashima Y, Plump AS, Raines EW, Breslow JL, Ross R. ApoE-deficient mice develop lesions of all phases of atherosclerosis throughout the arterial tree. *Arterioscler Thromb* 1994;14(1):133–140.
- Hitchens TK, Ye Q, Eytan DF, Janjic JM, Ahrens ET, Ho C. ^{19}F MRI detection of acute

- allograft rejection with in vivo perfluorocarbon labeling of immune cells. *Magn Reson Med* 2011;65(4):1144–1153.
28. Zhong J, Mills PH, Hitchens TK, Ahrens ET. Accelerated fluorine-19 MRI cell tracking using compressed sensing. *Magn Reson Med* 2013;69(6):1683–1690.
29. Pan H, Myerson JW, Hu L, et al. Programmable nanoparticle functionalization for in vivo targeting. *FASEB J* 2013;27(1):255–264.
30. Jacoby C, Temme S, Mayenfels F, et al. Probing different perfluorocarbons for in vivo inflammation imaging by 19F MRI: image reconstruction, biological half-lives and sensitivity. *NMR Biomed* 2014;27(3):261–271
31. Temme S, Bönner F, Schrader J, Flögel U. 19F magnetic resonance imaging of endogenous macrophages in inflammation. *Wiley Interdiscip Rev Nanomed Nanobiotechnol* 2012;4(3):329–343.
32. Ahrens ET, Flores R, Xu H, Morel PA. In vivo imaging platform for tracking immunotherapeutic cells. *Nat Biotechnol* 2005;23(8):983–987.
33. Rudd JH, Narula J, Strauss HW, et al. Imaging atherosclerotic plaque inflammation by fluorodeoxyglucose with positron emission tomography: ready for prime time? *J Am Coll Cardiol* 2010;55(23):2527–2535.
34. Srinivas M, Turner MS, Janjic JM, Morel PA, Laidlaw DH, Ahrens ET. In vivo cytometry of antigen-specific t cells using 19F MRI. *Magn Reson Med* 2009;62(3):747–753.
35. Tirota I, Mastropietro A, Cordiglieri C, et al. A superfluorinated molecular probe for highly sensitive in vivo(19)F-MRI. *J Am Chem Soc* 2014;136(24):8524–8527.